

See discussions, stats, and author profiles for this publication at: <https://www.researchgate.net/publication/51603058>

Assemblies of Functional Small-Sized Molecules Having 4-Amino-2,2,6,6-tetramethylpiperidine-1-oxyl Responsive to Heat and pH in Water and Their Water Proton Relaxivities

ARTICLE *in* LANGMUIR · AUGUST 2011

Impact Factor: 4.46 · DOI: 10.1021/la2029565 · Source: PubMed

CITATIONS

5

READS

21

4 AUTHORS, INCLUDING:



Satoru Karasawa

Kyushu University

60 PUBLICATIONS 977 CITATIONS

[SEE PROFILE](#)

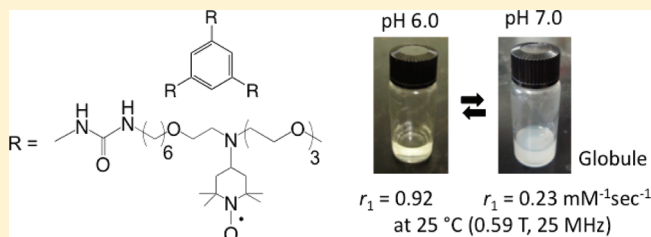
Assemblies of Functional Small-Sized Molecules Having 4-Amino-2,2,6,6-tetramethylpiperidine-1-oxyl Responsive to Heat and pH in Water and Their Water Proton Relaxivities

Hiroyuki Hayashi, Kengo Ohkubo, Satoru Karasawa, and Noboru Koga*

Graduate School of Pharmaceutical Sciences, Kyushu University, 3-1-1 Maidashi, Higashi-ku, Fukuoka 812-8582, Japan

Supporting Information

ABSTRACT: 1,3,5-Triureabenzene derivatives carrying alkyl (C_n) and poly(ethylene glycol) (Eg_m) chains C_nEg_3 (**1**, **2**, and **3**, $n = 6, 7$, and 8 , respectively) and $C_nN(X)Eg_m$ (**4** and **5**, $X = M$ (methyl), $n = 6$ and 8 , respectively, $m = 3$; **6** and 7 , $X = T$ (2,2,6,6-tetramethylpiperidine-1-oxyl, TEMPO), $n = 6$, $m = 3$ and 6 , respectively) were prepared. All compounds in aqueous solutions exhibited the lower critical solution temperature (LCST) phenomena unique for small-sized molecules and formed self-assemblies above the transition temperature, T_t , of the LCST. Only compound **3** formed a hydrogel with a minimum gelation concentration of 0.5 mM (0.05 wt %). In 1.0 mM aqueous solution, the T_t values were determined to be in the range of $12\text{--}40^\circ\text{C}$. In addition, the T_t values for **4**–**7** containing tertiary amine also responded to the solution pH with high sensitivity. The LCST behaviors for all compounds were reversible in the cycles of warming and cooling. The water proton relaxivities, r_1 , for **6** and **7** carrying TEMPO were altered below and above T_t and were largely reduced by the formation of self-assemblies above T_t . Compound **6** showed r_1 values at 25°C of 0.92 and $0.23\text{ mM}^{-1}\text{ s}^{-1}$ at pH 7.0 and 6.0, respectively. In transmission electron microscopy (TEM) images, globular particles with polydispersity were observed, and their average hydrodynamic diameters (D_H) were determined to be in the range of $2400\text{--}730\text{ nm}$ by dynamic light scattering. In the TEM and scanning electron microscopy images of a xerogel sample of **3**, bundles of fibers with a diameter of ca. 10 nm and a network structure, respectively, were observed.



$$r_1 = 0.92 \quad r_1 = 0.23\text{ mM}^{-1}\text{ sec}^{-1}$$

25°C (0.59 T, 25 MHz)

INTRODUCTION

Functional assemblies¹ including hydrogels, vesicles, and micelles responsive to external stimuli, heat,^{1b,c,2} light,³ pH,^{1b,4} and ion strength,⁵ etc., in water have been extensively studied for application as new functional soft materials, especially as carriers in the field of drug delivery systems (DDSs). One of the unique thermoresponsive behaviors would be a lower critical solution temperature (LCST) phenomenon^{6–8} in which the solution of a substance is clear at low temperatures and becomes turbid at high temperature. Since the aggregates above the LCST in the molecular system are of nano/micrometer size, they could potentially become nano/microsized functional materials responsive to heat.⁹ Substances already well-defined for the LCST are water-soluble polymers, poly(isopropylacrylamide) (NIPAAm) derivatives⁶ and their analogues,⁷ in which the LCST phenomena are known to be caused by coil–globule transition. In contrast, although the small-sized organic molecules which take advantage of the strategy of supramolecular self-assembly have also been developed,¹⁰ examples of observation of the LCST in nonpolymers are limited.^{3b,8b,11} Small-sized molecules¹² and modified dendrimers¹³ showing LCST phenomena have recently been reported. The small-sized molecules in mixtures of water and polar solvent were found to form assemblies above the LCST. However, observations of LCST phenomena in pure water are still rare. The advantage of

self-assembly consisting of small-sized molecules is that it would be relatively easy to modify the physical properties of assemblies and functionalize them by introducing the functional group to the starting molecules. In the present study, we attempted to prepare small-sized molecules with organic spins showing LCST phenomena in pure water and carried out the assembly of the organic spins by using the LCST phenomena for the new type of macromolecular magnetic resonance imaging (MRI) contrast agent.¹⁴ Recently, macromolecules and assemblies carrying chelated metal ions (mainly Gd³⁺) and stable radicals have been intensively studied as MRI contrast agents with targeting ability.¹⁵ For this purpose, we selected the 1,3,5-triureabenzene derivatives carrying amphiphilic side chains as the framework and carried out the construction of functional assemblies with organic spins. The molecules having analogous frameworks were already prepared, and their self-assembly behaviors in various solvents have been investigated in detail.^{1b,16,17} Accordingly, the 1,3,5-triureabenzene framework would be a useful building block for the construction of functional supramolecular self-assemblies in water. 4-Amino-2,2,6,6-tetramethylpiperidine-1-oxyl (amino-TEMPO) was

Received: July 28, 2011

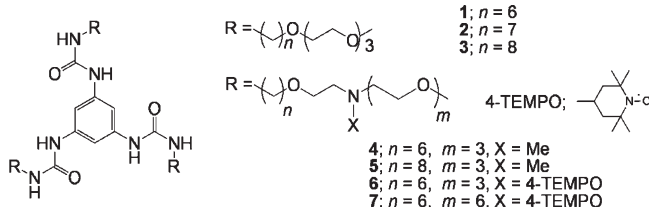
Revised: August 25, 2011

Published: August 29, 2011

used as an organic spin and was incorporated into the amphiphilic side chain of the supramolecule. The amine moiety of amino-TEMPO also introduces pH responsiveness, as reported in poly(amidoamine) (PAMAM) dendrimers.¹⁸ Therefore, the introduction of amino-TEMPO was expected to add two functions to LCST phenomena, magnetic resonance responsiveness and pH responsiveness by the resulting tertiary amine. In this study, 1,3,5-triureabenzene derivatives carrying the amphiphilic chains of alkyl and poly(ethylene glycol) groups and those containing the methylamine and amino-TEMPO units were prepared, and their self-assembly behaviors in response to heat and pH, magnetic properties, and morphology were investigated in water. All compounds successfully exhibited LCST phenomena in pure water. We report the preparation of functionalized 1,3,5-triureabenzene derivatives, their thermal and dual thermal–pH response behaviors in pure water, and the water proton relaxivity of TEMPO below and above the LCST.

■ RESULTS AND DISCUSSION

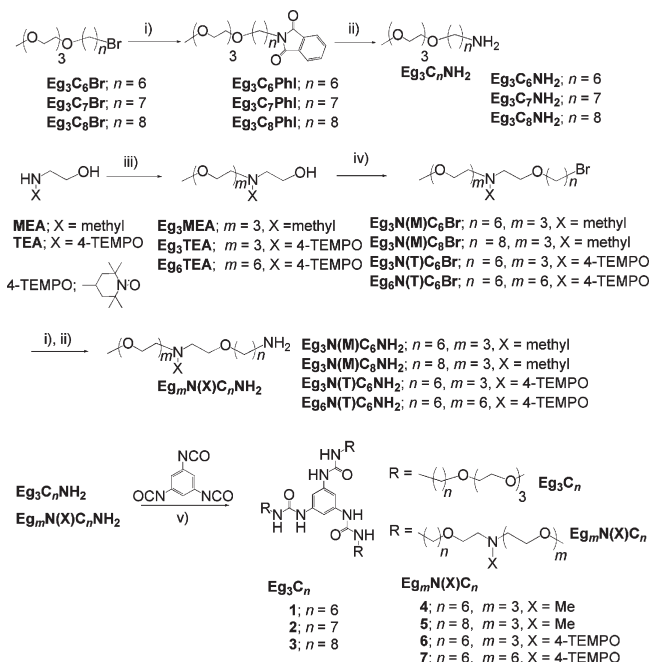
Design and Preparation of Molecules. In 1,3,5-triureabenzene derivatives carrying the amphiphilic chain C_nEg_m consisting of alkyl (C_n) and poly(ethylene glycol) (Eg_m) groups, the ratio of the lengths of the C_n and Eg_m chains is important for functionalization in water. Initially, to confirm the solubility of the molecules in water, the length of C_n was altered from $n = 6$ to $n = 8$ with a constant length of the Eg_3 chain and C_n employed as an amphiphilic side chain for **1**, **2**, and **3** (C_nEg_3 ; $n = 6, 7$, and 8 , respectively). On the basis of the obtained results of solubility of **1**–**3** in water, the lengths of C_n and Eg_m for the functional 1,3,5-triureabenzene derivatives $C_nN(X)Eg_m$ (**4** and **5**, $X = M$ (methyl), $n = 6$ and 8 , respectively, $m = 3$; **6** and **7**, $X = T$ (TEMPO), $n = 6, m = 3$ and 6 , respectively) were determined, and additional functional units, methylamine for **4** and **5** and amino-TEMPO for **6** and **7**, were incorporated between the C_n and Eg_m chains.



These compounds had C_3 symmetry and consisted of four functional groups, the benzene ring for $\pi-\pi$ interaction, the urea groups for hydrogen bonding, the C_n chain for hydrophobic interaction, and the Eg_m chain for solubility in water and thermal responsiveness. Compounds **4**–**7**, having molecular structures similar to those for **1**, **2**, and **3**, introduced additional functions, pH responsiveness for **4** and **5** and both magnetic resonance responsiveness and pH responsiveness for **6** and **7**. Preparation routes of compounds **1**–**7** are shown in Scheme 1, and details for the preparation are described in section S1 in the Supporting Information.

1,3,5-Triureabenzene derivatives carrying amphiphilic side chains were prepared by the coupling reaction of 1,3,5-benzenetriisocyanate¹⁹ generated in situ with TEG-alkylamine, $Eg_3C_nNH_2$, and PEG-X-alkylamine, $Eg_mN(X)C_nNH_2$ ($X = M$ and T for methyl and TEMPO, respectively). $Eg_3C_nNH_2$ were prepared by the standard procedure reported previously.¹⁷ $Eg_3N(X)C_nNH_2$ was prepared in a manner similar to the procedure for $Eg_3C_nNH_2$.

Scheme 1. Preparation Routes of Compounds **1**–**7**



by using *N*-methylethanolamine and *N*-TEMPO-ethanolamine, which was obtained by the reductive amination of oxo-TEMPO with $\text{NaB}(\text{CN})\text{H}_3$ in the presence of ethanolamine. Although in Gabriel synthesis for $Eg_3N(T)C_nNH_2$ TEMPO radicals were reduced to hydroxylamine by the reduction with hydrazine hydrate, they were easily and quantitatively recovered by oxidation with oxygen bubbling under basic conditions.

The compounds were obtained as colorless gummy solids for **1**, **2**, and **3**, a pale yellow oil for **4** and **5**, and an orange oil with high viscosity for **6** and **7**. The compounds except for **3** were readily soluble in water at low temperature (ca. 4 °C), while **3** was less soluble without preheating. After the mixture of **3** and water was heated at ca. 90 °C and rapidly cooled to near 0 °C, **3** was soluble to more than 5.0 mM (~0.5 wt %) under sonication. Without preheating, the limit of the solubility was ca. 1.0 mM.

Self-Assembly Behaviors. In aqueous solutions, all compounds except for **3** showed similar thermal behaviors in response to heat. The aqueous solutions were transparent at low temperature and on warming became turbid (Figure 1a), indicating that these compounds exhibited LCST phenomena. In **4**–**7** containing the tertiary amine unit, additionally, the LCST behaviors were also controlled by the pH of the solution and the transition temperature, T_g , as the LCST shifted to a higher value with decreasing pH. The observed LCST behaviors might be caused by the entropically favorable dehydration due to the Eg_m chain. In contrast, the clear solution of **3** dissolved in water at 4 °C gradually became a hydrogel (~15 min) at 20 °C (i and ii in Figure 1b). On warming, the resulting clear hydrogel became turbid at 30 °C (iii in Figure 1b) and started to shrink due to a phase separation above 39 °C (iv in Figure 1b). The minimum gelation concentration (MGC) was 0.5 mM (0.05 wt %), which is rather low compared with those of other hydrogelators of low molecular weight.²⁰ The observed thermal responsive behavior for the hydrogelation was the opposite of that for usual gelators, which dissolve at high temperature and form a gel at low temperature. The LCST behaviors for all compounds were

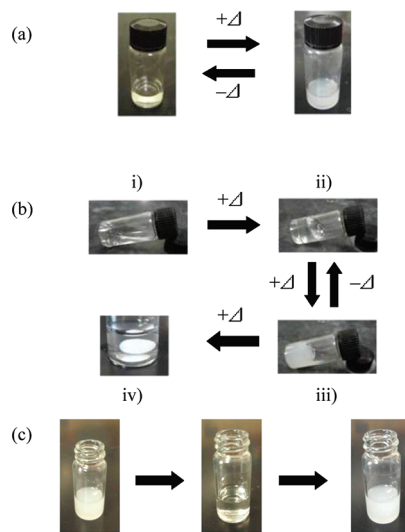


Figure 1. Photographs of the vial for a 1 mM aqueous solution of (a) **1** at ca. 20 °C (left) and at ca. 40 °C (right), (b) **3** at near 4 (i), 20 (ii), 35 (iii), and 40 (iv) °C, and (c) **6** at 25 °C at pH 7.0 (left) and in the acidic (middle) and basic (right) solutions.

reversible in the cycles of warming and cooling, while the formation of hydrogel by **3** was irreversible. In the solutions of **4–7**, the clearance and turbidity were repeated by the cycle of acidic and basic conditions at constant temperature. The views of the change of solution for **6** at 25 °C in acidic and basic conditions are shown in Figure 1c.

Determination of the Transition Temperature for the LCST. The transmittance at 800 nm, Tr_{800} , for the aqueous solution samples (1.0 mM) was measured on warming (sweep rate 1 °C/min) in the temperature range of 5–50 °C. The solutions at low temperature were clear. On warming, the values of Tr_{800} were 100% until a certain temperature and then abruptly decreased, indicating that the solution became turbid. The temperature dependences of Tr_{800} are shown in Figure 2a for **1**, **2**, and **3** and Figure 2b for **4**, **5**, **6**, and **7**. The temperature at which the Tr_{800} value started to decrease was defined as the transition temperature, T_t , of the LCST. From the plots of Tr_{800} vs T , the values of T_t were determined to be 33, 18, and 30 °C for **1**, **2**, and **3**, respectively, and 40, 34, 12, and 40 °C, for **4**, **5**, **6**, and **7**, respectively. The T_t values for the molecules depended on the solubility in water and shifted to a higher value with increasing solubility. In the sets of **1–3** and **4** and **5** having the same Eg_3 units, the solubility in water would decrease with increasing number of n in C_n . Therefore, the T_t values would be in the order of **1** > **2** > **3** and **4** > **5**. The obtained T_t values were consistent with the solubility of the molecules except for **3**. The T_t value of **3** was higher than that of **2**, indicating that the pathway to the turbidity of the hydrogel of **3** might be different. In Figure 2b, the thermal profile of Tr_{800} for **4** was different from the others and Tr_{800} gradually decreased above the temperature of 40 °C. At concentrations over 3 mM, however, Tr_{800} abruptly decreased at the same temperature. These results indicated that the thermal profile of Tr_{800} for **4** showed the concentration dependence. In **6** and **7** having C_6 units, the solubility would increase with increasing number of m in Eg_m . In fact, the T_t value of **6** was higher than that of **7**.

To investigate the concentration dependence of T_t , the temperature dependence of Tr_{800} was also measured in the concentration range of 5.0–0.2 mM. The T_t values for **1**

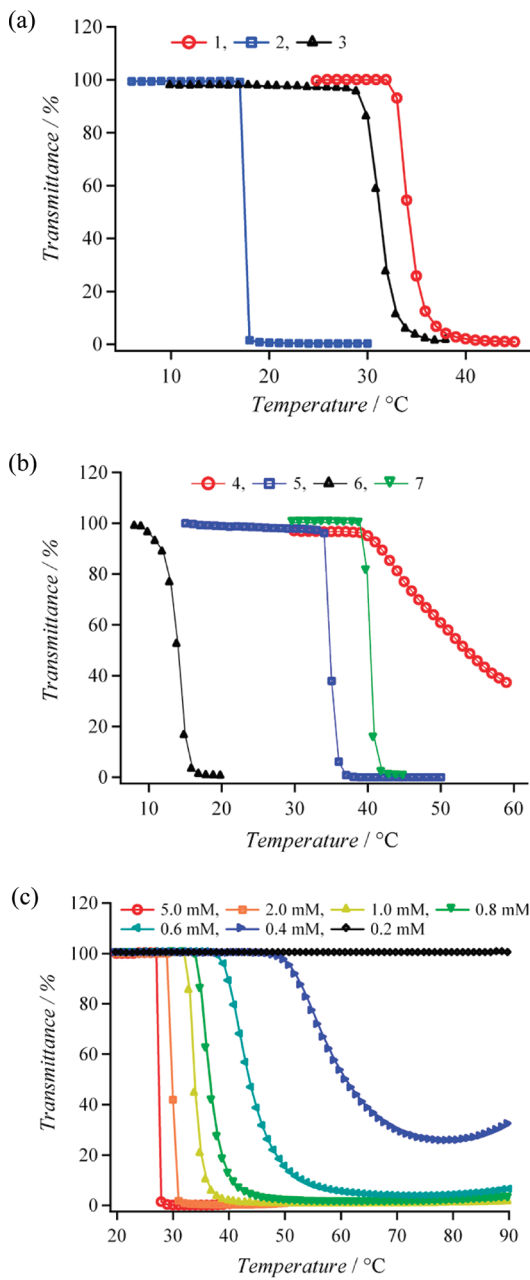


Figure 2. Tr_{800} vs T in a 1 mM solution of (a) **1** (red circles), **2** (blue squares), and **3** (black triangles) and (b) **4** (red circles), **5** (blue squares), **6** (black triangles), and **7** (green inverted triangles) and (c) for **1** at various concentrations in the range of 5.0–0.2 mM.

depended on the concentration, and the Tr_{800} vs T plots at various concentrations for **1** are shown in Figure 2c. At concentrations of less than 1.0 mM, the T_t values largely shifted to high temperature with decreasing concentration, while in the concentration range of 5.0–1.0 mM the change of Tr_{800} and the degree of shift of T_t became sharp and small, respectively. The T_t values for 5.0, 2.0, 1.0, 0.8, 0.6, and 0.4 mM were 28, 30, 33, 39, 43, and 52 °C, respectively, and no decrease of Tr_{800} at 0.2 mM was observed below 90 °C. Similarly, in the other compounds, relatively small concentration dependences of T_t were observed at concentrations higher than 1 mM. In 5.0, 3.0, and 1.0 mM solution, the T_t values for **2** were 16, 16, and 18 °C, respectively,

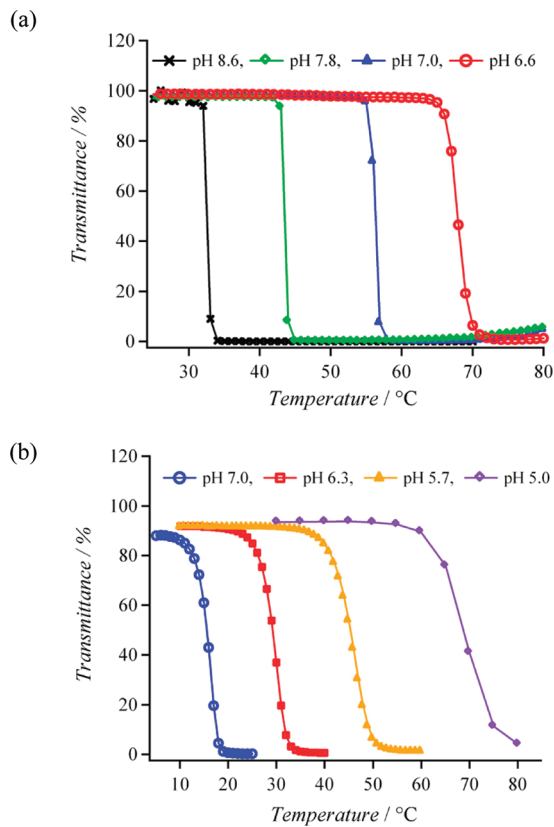


Figure 3. Tr_{800} vs T for **5** (a) and **6** (b) at the given pH values.

and those for **4**, **5**, **6**, and **7**, were nearly constant at 40, 34, 12, and 40 °C, respectively. In all compounds, the change of Tr_{800} became sharper with increasing concentration.

The pH dependence of T_t values for all compounds except **3** were examined in near-neutral conditions. The solutions in 100 mM phosphate buffer at pH 8.6, 7.8, 7.0, and 6.6 for **4** and **5** (3.0 mM) and at pH 7.0, 6.3, 5.7, and 5.0 for **1**, **2**, **6**, and **7** (1.0 mM) were used as samples, and Tr_{800} at the given pH values were measured in the temperature range of 10–90 °C. The T_t values for **1** and **2** were insensitive to the pH and nearly constant (25–28 and 13 °C, respectively), while those for **4**–**6** largely depended on the pH and increased with decreasing pH. The values for **1** and **2** in buffer solution were small compared with that of pure water, suggesting that they had salt effects. The T_t values at pH 8.6, 7.8, 7.0, and 6.6 were 38, 40, 70, and >90 °C for **4** and 32, 43, 55, and 65 °C for **5**, respectively, and those at pH 7.0, 6.3, 5.7, and 5.0 were 10, 25, 40, and 60 °C for **6**, respectively. The plots of Tr_{800} vs T at the given pH for **5** and **6** are shown in Figure 3 (4 in Figure S1, Supporting Information), and the values of T_t for **4**, **5**, and **6** are listed in Table 1. The fact that **1** and **2** did not show pH dependence of the T_t values, while **4**–**7** did, indicated that the observed pH dependence of T_t might be due to the tertiary amine units contained in **4**–**7**. The solubility of **4**–**7** in water was increased by the protonation of amino groups under acidic conditions, leading to the high value of T_t . The response of T_t for **5** and **6** was highly sensitive to the pH of the solution.

The LCST phenomenon of alternate clear and turbid states reversibly took place by the cycles of warming and cooling (above and below T_t). In addition, the pH dependence of T_t means that at a constant temperature it was possible to repeat the clear and

Table 1. pH Dependence of the LCST for **4, **5**, and **6****

	T_t of the LCST (°C)						
	pH 5.0	pH 5.8	pH 6.6	pH 7.0	pH 7.8	pH 8.6	
4				>90	70	40	38
5				65	55	43	32
6	60	40	25 (6.3) ^a	10			

^a The number in parentheses is the pH value.

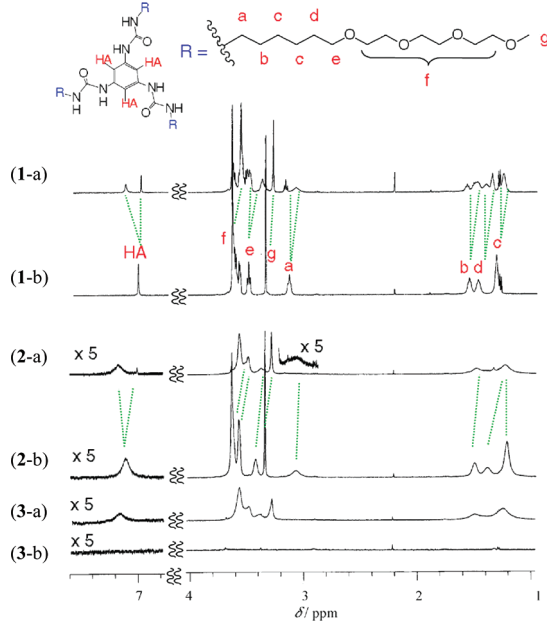


Figure 4. VT ^1H NMR spectra (500 MHz, D_2O with 4,4-dimethyl-4-silapentane-1-sulfonic acid (DSS) as a reference) of 1 mM solutions of **1** at 50 (1-a) and 10 (1-b) °C, **2** at 30 (2-a) and 10 (2-b) °C, and **3** at 35 (3-a) and 10 (3-b) °C. Labels a–h indicate assignment results of the protons in the alkyl and Eg_3 chains in **1**.

turbid states by pH alteration (Figure 1c). As expected from Figure 3b, the solution of **6** at 25 °C became clear at pH 6.0 and turbid at pH 7.0. It was confirmed that the clear–turbid states were repeated by cycles of pH 6.0 and 7.0. The reversible change of clear and turbid for hydrogel **3** was also observed by repeating the temperature cycle between 10 and 35 °C, as shown in Figure S2, Supporting Information.

Variable-Temperature (VT) ^1H NMR and Electron Spin Resonance (ESR) Measurements. VT ^1H NMR for **1, **2**, **3**, **4**, and **5**.** VT ^1H NMR experiments of 1.0 mM aqueous solutions were performed every 5 °C from 5 to 60 °C for **1**, **2**, and **3** and every 10 °C from 10 to 60 °C for **4** and **5** (Figure S3, Supporting Information). In VT ^1H NMR spectra, drastic changes were observed at a certain temperature close to T_t determined by the temperature dependence of the transmittance of Tr_{800} . The ^1H NMR spectra for **1**, **2**, and **3** and for **4** and **5** at temperatures below and above T_t are shown in Figures 4 and 5, respectively.

In the spectrum for **1** at 5–30 °C, all signals were sharp and no broadening was observed, indicating that compound **1** existed as a monomer without the formation of any assembly below 30 °C. The signals at 7.02, 3.64, 3.58, 3.35, 3.15, 1.56, 1.48, and 1.32 ppm were assigned as H_A , H_B , H_E , H_G , H_A' , H_B' , H_D , and H_C .

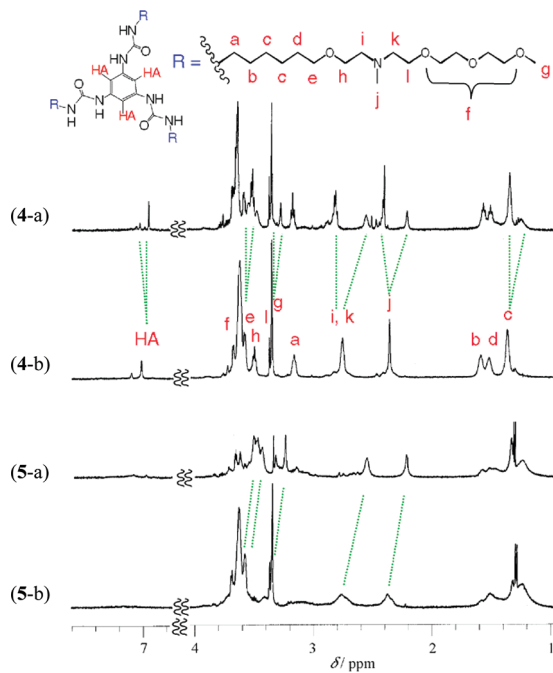


Figure 5. VT ^1H NMR spectra (500 MHz, D_2O with 4,4-dimethyl-4-silapentane-1-sulfonic acid (DSS) as a reference) of 1 mM solutions of **4** at 60 (4-a) and 10 (4-b) °C and **5** at 50 (5-a) and 10 (5-b) °C. Labels a–l indicate assignment results of the protons in the alkyl and Eg_3 chains in **4**. The dotted lines indicate the chemical shifts for new peaks appearing above T_t .

respectively, and are shown in panel 1-b of Figure 4. At 35 °C, a new set of broad signals appeared at 7.15, 3.48, 3.38, 3.30, 3.08, 1.57, 1.34, and 1.24 ppm as shown in panel 1-a of Figure 4, and on warming, those signal intensities increased at the expense of the sharp signals. Since the temperature of 35 °C revealed new signals and was close to the T_t value for **1** (Figure 2a), the new broad signals were presumably due to the self-assemblies formed at 35 °C, and this amount and/or size gradually increased above T_t . In the spectra above 35 °C, the signal for the benzene proton (H_A) shifted to low field, while those assigned as alkyl and PEG units shifted to high field. The deshielding of the H_A proton and the shielding of the side-chain protons might be due to the formation of an intramolecular hydrogen bond between the carbonyl in the urea moiety and the H_A proton caused by the alteration of the circumstance of the hydration in the assembly and the closed contacts of the side chain by the intermolecular hydrophobic interaction, respectively. Similar signal changes were observed in the assembly of analogous molecules.²¹ The ratio $I_{7.15}/I_{7.02}$ ($I_{7.15}$ and $I_{7.02}$ are the intensities of the signals at 7.15 and 7.02 ppm, respectively) of the broad to the corresponding sharp signals obtained by the integration of both peaks was 0.62. On warming, the ratio increased and reached 2.64 at 60 °C, indicating that the amount and/or size of the assembly increased with increasing temperature. Interestingly, the value of 2.64 corresponded to the monomer of 0.27 mM, which was consistent with the result of the concentration dependence of the transmittance (Figure 2c). The spectra for **2** at 5 and 10 °C showed broad signals at 7.11, 3.58, 3.43, 3.08, and 1.22 ppm, which were assigned as H_{A} , H_{B} , H_{e} , H_{a} , and H_{c} protons, respectively. Those chemical shifts were not consistent with those for **1** either below or above T_t and were located between those of the monomer and the assembly for **1**. These spectra might suggest the formation of

a certain assembly. At 20 °C, the spectrum drastically changed and all signals shifted. The resulting spectrum was close to that of the assembly for **1**, including the small amount of monomer. Notably, the signal at 7.11 ppm for H_{A} at 5 and 10 °C split into two signals at 7.15 and 7.02 ppm at 20 °C, which were consistent with those assigned as H_{A} in the assembly and the monomer of **1**, respectively. Since the solution was clear at 5 and 10 °C, the assembly that formed below 20 °C might be different from the one above 20 °C and was suggested to be small-sized oligomers. On warming, the new signal intensity increased. The signal intensity ratio $I_{7.15}/I_{7.02}$ was 2.43 at 20 °C and reached 21.4 at 40 °C, as shown in Figure S3, Supporting Information, indicating that the amount and/or size of the assembly increasing with increasing temperature above T_t was also the case for **1**. In the spectrum for compound **3**, no significant signals were observed at 5–30 °C, and then broad signals at 7.15, 3.53, 3.08, 1.51, and 1.24 ppm suddenly appeared at 30–35 °C. The observed spectrum at 35 °C was very similar to those for **1** and **2** above T_t , and the temperature of 30 °C was consistent with the one at which turbidity was observed in **3**. These spectral changes indicated that the motion of molecule **3** was suppressed in the range of 5–30 °C by the formation of the hydrogel structure. Since the hydrogel was still maintained at 30–35 °C as shown in Figure 1b, the appearance of the signals assigned as the assemblies might be due to the beginning of the decomposition of the gel structure in the hydrogel. The hydrogel partially decomposed to the monomer or oligomer, which were immediately affected by dehydration due to the Eg_3 groups to form globules in the hydrogel framework. Compound **3** was anticipated to have a T_t value lower than that (12 °C) of **2**. It is noted that no signals due to the monomer and the oligomer were observed below 30 °C, indicating that the turbidity observed above 30 °C was not derived from them.

In the spectra of **4** in the temperature range of 30–10 °C (below T_t), sharp signals were observed and assigned as shown in panel 4-b of Figure 5. The spectra also showed a weak broad signal at 7.12 ppm in a signal intensity ratio $I_{7.12}/I_{7.03}$ of 0.37 in addition to sharp signals, suggesting that compound **4** mainly existed as a monomer containing a small amount of assembly, which might be an oligomer. At 40 °C, new weak signals at 7.10, 3.35, 3.22, 2.56, and 2.21 ppm appeared in addition to the signals due to the monomer. The signals assigned as methylene and methyl protons (H_i and H_k , and H_j , respectively) neighboring the nitrogen of the amine at 2.75 and 2.38 ppm shifted to 2.56 and 2.22 ppm and were clearly observed, indicating that the assembly formed above 40 °C. The signal intensity ratios for $I_{2.56}/I_{2.75}$ and $I_{2.22}/I_{2.38}$ at 40 °C were 0.10 and 0.13, respectively, and on warming, those values gradually increased. The observed relationship between the increase of assembly and the temperature, that the assembly slightly formed in the range of 40–60 °C, was in good agreement with the result for the thermal profile of Tr_{800} , in which the Tr_{800} value for the sample of the 1.0 mM solution gradually decreased above 40 °C (Figure 2b). In contrast, the spectra for **5** at 10–30 °C (below T_t) were similar to those for **4** below T_t , in which the protons of H_{A} , H_{a} , and H_{h} were extremely broad and $\text{H}_{\text{i},\text{k}}$ and H_{j} were also broad compared with those for **4** below T_t . The observed broadness of the signals for benzene and the alkyl chain might suggest the formation of a small-sized oligomer. Above 40 °C (above T_t), new signals at 3.35, 3.25, 2.56, and 2.22 ppm appeared at the expense of old ones. Those chemical shifts were consistent with the corresponding shifts for **4** above T_t .

The observed thermal profiles of NMR spectra below and above T_t in 1 mM solutions indicated that, in the 1 mM aqueous solution of the molecules, equilibria among the monomer, the oligomer, and the self-assembly were established. Below T_t , the molecules were predominantly monomers for **1** and **4** and oligomers for **2** and **5**, while above T_t the equilibrium for **1** and **4** gave a mixture of the monomer and the assembly and those for **2** and **5** mainly leaned toward the assemblies. These results suggested that the compound with lowering T_t predominantly existed as an oligomer below T_t and as the assembly above T_t .

ESR Spectra for **6 and **7**.** ESR spectra ($\nu_0 = 9.4$ GHz) of the solutions (1 mM) of **6** and **7** in water were measured in the temperature range of 10–50 °C. TEMPO-OH, 4-hydroxy-2,2,6,6-tetramethylpiperidine-1-oxyl, was also measured under conditions similar to those of a reference compound. The temperature dependences of ESR spectra for **6** are shown in Figure 6a (7 and TEMPO-OH in Figure S4a,b, Supporting Information). The spectra at 10 °C (less than T_t of 12 and 39 °C for **6** and **7**, respectively) for both compounds were similar to each other and showed broad three-line signals with $g = 2.0068$ and 2.0068 and hyperfine coupling constant $a_N = 16.1$ and 16.2 G due to the nitrogen nuclei for **6** and **7**, respectively. The line widths, ΔH_{pp} , from the top to the bottom of the peak of the center signal, were 4.1 and 3.1 G for **6** and **7**, respectively, at 10 °C. In the spectra, anisotropic broadenings in the high-field line were observed. According to Kivelson's equation,^{14b,22} the rotational correlation time, τ_R , was estimated from the spectra at 10 °C, and τ_R values of 7.5×10^{-10} and 7.9×10^{-10} s for **6** and **7**, respectively, were obtained. Those τ_R values were ca. 20 times longer than that (0.4×10^{-10} s) for TEMPO-OH obtained under similar conditions. Broad spectra with slow rotation of the aminoxy center suggested that the oligomers formed and the intra- and/or intermolecular spin–spin interaction took place between the aminoxy centers. On warming, the shapes of the spectra for **6** and **7** gradually changed with decreasing intensity and line width (ΔH_{pp}) of the three-line signal (Figures 6a and S4a), becoming spectra with a broad one-line signal and a sharp three-line one at 40 and 50 °C, respectively. In the ESR spectra for **6**, although no abrupt changes of the spectra near T_t (10–20 °C) were observed, the height and width of the center signal of the three-line signal largely decreased with increasing temperature (Figure S4c,d). Since the effect of the Curie law on the signal intensity was small in the temperature region of 0–40 °C, the actual signal intensity change for TEMPO-OH in the range of 0–40 °C was small (Figure S4b), and the large decrease in the height and width of the signal suggested the formation of a broad one-line signal, which might be due to the assembly. In contrast, **7** showed changes to the spectra consisting of a broad one-line signal with a sharp three-line signal near T_t (40–50 °C in Figure S4a). The temperature dependence of ESR spectra for **6** and **7** in 1 mM solution suggested that, below T_t , the oligomers were dominant in the equilibrium between the monomer and the oligomer, while above T_t mixtures of the assembly and the monomer were produced. From the simulation of the spectra at 40 and 50 °C for **6** and **7**, the ratios of the assembly and the monomer were estimated to be 0.01 and less than 0.01, respectively.

The solutions (1 mM) of **6** in 100 mM phosphate buffer at pH 7.0 and 6.0 were used, and ESR spectra were measured at 25 °C. The sample solutions at 25 °C were turbid at pH 7.0 and clear at pH 6.0, as expected from the results of the pH dependence of T_{r800} at 25 °C (Figure 3b). ESR spectra at pH 7.0 and 6.0 at

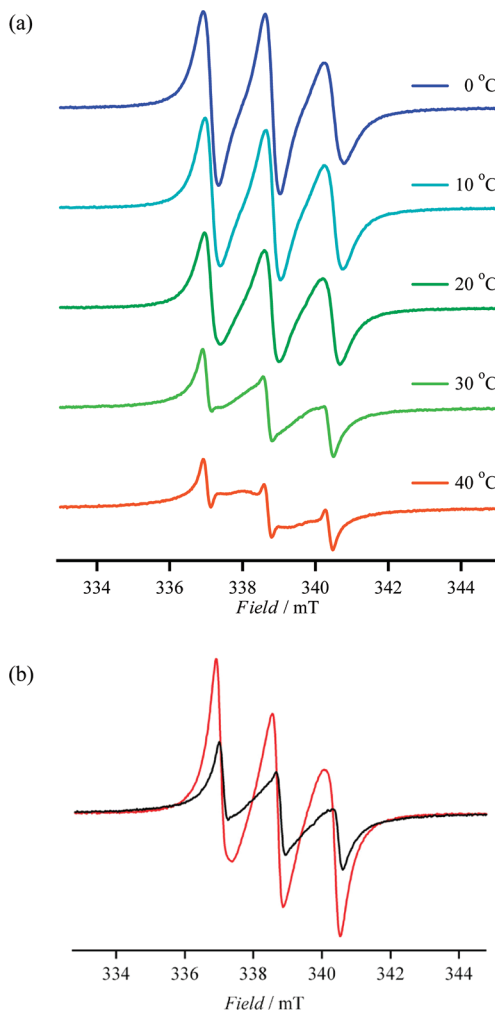


Figure 6. ESR spectra ($\nu_0 = 9.4$ GHz) of the solution (1.0 mM) of **6** (a) at various temperatures and (b) at 25 °C and at pH 7.0 (black) and 6.0 (red).

25 °C are shown in Figure 6b. The spectra at pH 7.0 and 6.0 were similar to those at 10 and 30 °C, respectively, as seen in Figure 6a. Although the obtained spectra at both pH values showed three-line signals similar to each other, the height and width of the center signal in the three-line signal at pH 6.0 were higher by 2.3- and 1.6-fold, respectively, than those at pH 7.0. It was confirmed by the double integral of the ESR signal that the amounts of spin for both spectra were the same. This result indicated that the contribution of the broad one-line signal due to the assembly in the spectrum at pH 7.0 was larger than that at pH 6.0.

The observed thermal and pH profiles of ESR spectra for **6** and **7** suggested that the local circumstances of the aminoxy centers were not largely changed above T_t . In other words, the molecules in the assemblies would be loosely assembled.

Relaxivity Measurements. The solutions (0.0, 1.3, 2.0, 2.6, and 3.2 mM) of **6** and **7** in pure water were used as samples, and the spin–lattice relaxation rates, T_1^{-1} , were measured in the temperature ranges of 5–25 °C for **6** and 25–55 °C for **7** by a ^1H pulse NMR spectrometer (0.59 T, 25 MHz). In these concentration ranges, similar clear–turbid solution changes were observed at 12 and 40 °C for **6** and **7**, respectively. The solution of TEMPO-OH was used as a reference sample, and the values of T_1^{-1} were also measured in the temperature range of 5–55 °C

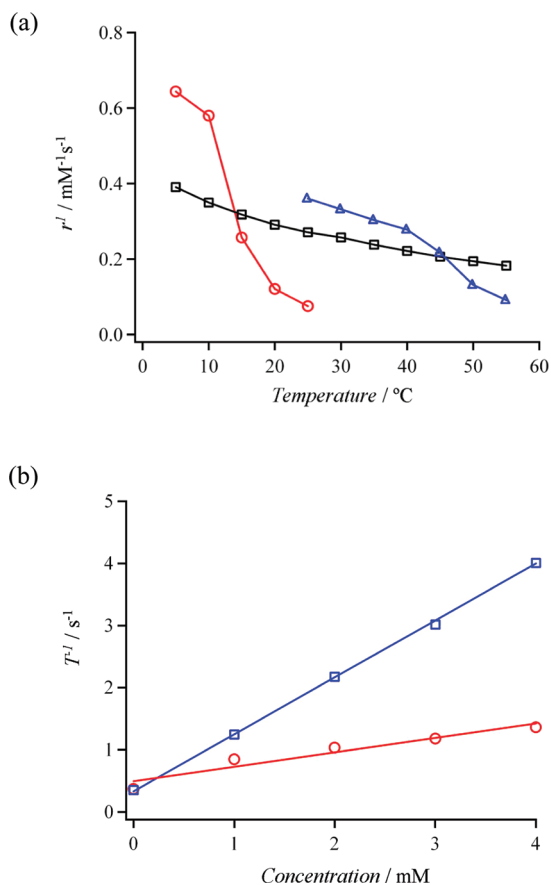


Figure 7. (a) r_1 per aminoxylo vs T for **6** (red circles), **7** (blue triangles), and TEMPO-OH (black squares) and (b) T_1^{-1} vs concentration for **6** at pH 6.0 (red circles) and 7.0 (blue squares) at 25 $^\circ\text{C}$.

under similar conditions. In the plots of T_1^{-1} vs concentration at each temperature, the values of T_1^{-1} increased proportionally. The linear relationship indicates that the influence of the concentration on the equilibrium state in this range of 1.3–3.2 mM was insignificant. The relaxivity values, r_1 , obtained from the concentration dependence of T_1 were 1.9, 1.7, 0.78, 0.36, and $0.24 \text{ mM}^{-1} \text{ s}^{-1}$ at 5, 10, 15, 20, and 25 $^\circ\text{C}$ for **6** and 1.1, 0.99, 0.90, 0.84, 0.66, 0.39, and $0.27 \text{ mM}^{-1} \text{ s}^{-1}$ at 25, 30, 35, 40, 45, 50, and 55 $^\circ\text{C}$ for **7**, respectively. The obtained r_1 values for **6** and **7** were combined with those for TEMPO-OH and were plotted as a function of the temperature. The plots of r_1 per aminoxylo vs T for **6**, **7**, and TEMPO-OH are shown in Figure 7a. In the temperature dependence of the relaxivities for **6** and **7**, on warming, the values of r_1 largely decreased at temperatures near T_t (12 and 40 $^\circ\text{C}$ for **6** and **7**, respectively), while those for TEMPO-OH as a reference molecule gradually decreased in the range of 5–55 $^\circ\text{C}$. The r_1 values per aminoxylo for **6** at 5 and 10 $^\circ\text{C}$ below T_t were 0.64 and $0.58 \text{ mM}^{-1} \text{ s}^{-1}$, respectively, while those at 20 and 25 $^\circ\text{C}$ above T_t were 0.12 and $0.08 \text{ mM}^{-1} \text{ s}^{-1}$, respectively. The obtained values below T_t were quite large compared with those for TEMPO-OH (0.39 and 0.35 at 5 and 10 $^\circ\text{C}$, respectively), and those above T_t were smaller than those for TEMPO-OH (0.29 and 0.27 at 20 and 25 $^\circ\text{C}$, respectively). Below T_t (12 $^\circ\text{C}$), the molecules would be a mixture of isolated monomers and small-sized oligomers and would show a large r_1 . Since the r_1 value was closely related to the rotational correlation time, τ_R ,^{14b,23} the large r_1 values compared with those for

TEMPO-OH at 5 and 10 $^\circ\text{C}$ might have been caused by the large τ_R value due to the molecular size of a monomer or an oligomer. In a 1 mM solution of **6**, actually, the τ_R value obtained by ESR spectroscopy was $7.5 \times 10^{-10} \text{ s}$, which was ca. 20 times longer than that for TEMPO-OH. In addition, the increase in the amount of water molecules by hydrating TEG side chains might affect the large r_1 value. Above T_t , on the other hand, the molecules of the monomers and/or the oligomers formed assemblies due to dehydration (lack of water molecules) and the r_1 value largely decreased. It was considered significant for reduction of the r_1 that the limitation of the contact between the aminoxylo and water molecules in the assembly formed by dehydration and exchange of water molecules around aminoxylo in the assembly with bulk water became slow. Those factors might predominate the effect of the increase in τ_R caused by the increase of the molecular weight by forming the assembly. Similar decreases of the relaxivity were observed in dendrimers, micelles, and vesicles containing paramagnetic species.²⁴ The r_1 value at 10 $^\circ\text{C}$ is 5 times larger than that at 20 $^\circ\text{C}$. In the temperature dependence of r_1 values for **7**, the change of the r_1 values below and above T_t was also observed. The r_1 values for **7** at 25 and 35 $^\circ\text{C}$ below T_t (40 $^\circ\text{C}$) were 0.36 and $0.30 \text{ mM}^{-1} \text{ s}^{-1}$, respectively, while those at 50 and 55 $^\circ\text{C}$ above T_t were 0.13 and $0.09 \text{ mM}^{-1} \text{ s}^{-1}$, respectively. The observed thermal behavior of r_1 for **7** was considered in a manner similar to that for **6**.

Subsequently, the pH dependence of r_1 for **6** was investigated at a constant temperature, 25 $^\circ\text{C}$. The spin-lattice relaxation rate, T_1^{-1} , of the solution samples (0.0, 1.0, 2.0, 3.0, and 4.0 mM) at pH 7.0 and 6.0 in 100 mM phosphate buffer were measured at 25 $^\circ\text{C}$. Since the T_1 values at pH 7.0 and 6.0 for **6** were 10 and ca. 40 s , respectively (Figure 3b), the solution samples at 25 $^\circ\text{C}$ were turbid at pH 7.0 and clear at pH 6.0. (Figure 6b). The plot of T_1^{-1} vs concentration at pH 7.0 and 6.0 is shown in Figure 7b. From the slope in the T_1^{-1} vs concentration plot, the r_1 values were estimated to be 0.23 (0.08) and 0.92 (0.31) $\text{cm}^{-1} \text{ s}^{-1}$ at pH 7.0 and 6.0, respectively, in which the values in parentheses are per aminoxylo. The r_1 value per aminoxylo at pH 6.0 was slightly larger than that (0.28) for TEMPO-OH, and 4 times larger than that at pH 7.0 and 25 $^\circ\text{C}$. The difference in r_1 at pH 6.0 and 7.0 was explained as the decrease in the r_1 value caused by the formation of the assembly.

Size and Morphology of Self-Assemblies. The solutions (10 mM for **1**, **2**, and **6** and 5 mM for **4** and **5**) of the compounds except for **3** dissolved in water after filtration with a membrane filter of diameter $0.45 \mu\text{m}$ were used as the samples for dynamic light scattering (DLS) measurement. DLS was measured below and above T_t . Below T_t , scattering peaks were observed at sizes of less than 10 nm, while above T_t the broad peaks showing polydispersity were observed at sizes larger than 1000 nm. The average hydrodynamic diameters (D_H) were 4.1 ± 0.4 , 5.7 ± 0.7 , 3.6 ± 0.4 , 6.0 ± 0.6 , and 2.8 ± 0.4 nm at 10 $^\circ\text{C}$ for **1**, **2**, **4**, **5**, and **6**, respectively, and 2300 ± 600 nm at 35 $^\circ\text{C}$ for **1**, 2400 ± 500 nm at 25 $^\circ\text{C}$ for **2**, 2400 ± 300 nm at 50 $^\circ\text{C}$ for **4**, 1100 ± 190 nm at 70 $^\circ\text{C}$ for **5**, and 730 ± 140 nm at 25 $^\circ\text{C}$ for **6**. The values below and above T_t might be due to the oligomer and the assembly, respectively. The obtained D_H values were significantly different, indicating that the size of the assemblies forming in water depended on the side chain. The results of DLS size distributions of **1**, **2**, **4**, **5**, and **6** are shown in Figure 8, and the D_H values are summarized in Table 2 together with the T_t values of the LCST. To investigate the pH dependence of the size at constant temperature, the phosphate buffer solutions of **5** at pH

7.0, 7.8, and 8.6 were measured at 37 °C (Figure 8c). As shown in Figure 3a, the solutions of **5** at 37 °C and at pH 7.0, 7.8, and 8.6

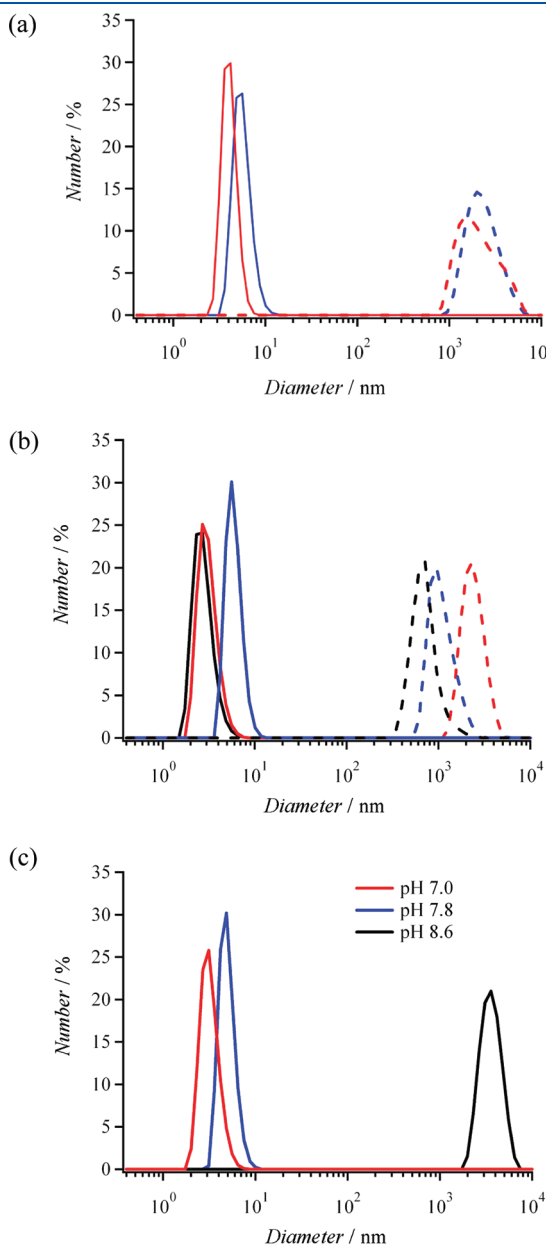


Figure 8. Size distributions in DLS in 10 mM aqueous solutions of (a) **1** (red) at 10 and 35 °C and **2** (blue) at 10 and 25 °C and (b) **4** (red) at 10 and 50 °C, **5** (blue) at 10 and 70 °C, and **6** (black) at 10 and 25 °C, in which the former and the latter temperatures were below (solid line) and above (dotted line) T_t , respectively, and (c) **5** at pH 7.0 (red), 7.8 (blue), and 8.6 (black) at 37 °C.

Table 2. D_H and T_t Values for **1**, **2**, **4**, **5**, and **6**^a

1	2	4	5	6
33	18	40	34	12
T_t of LCST (°C)				
4.1 ± 0.4 (10)	5.7 ± 0.7 (10)	3.6 ± 0.4 (10)	6.0 ± 0.6 (10)	2.8 ± 0.4 (10)
2300 ± 600 (35)	2400 ± 500 (25)	2400 ± 300 (50)	1100 ± 190 (70)	730 ± 140 (25)

^a The numbers in parentheses are the temperatures for DLS measurement.

were expected to be clear, clear, and turbid, respectively. The D_H values were 3.3 ± 0.4 , 5.0 ± 0.5 , and 3700 ± 470 nm at pH 7.0, 7.8, and 8.6, respectively. The size of the assembly formed at pH 8.6 was large compared with that in pure water, indicating that the size of the assembly depended on the salt concentration dissolved in water.

The results of DLS measurements at high concentration suggested that, in the equilibrium of the monomers, oligomers, and assemblies, the molecules predominantly existed as small assemblies of 3–6 nm below T_t and formed assemblies of 700–2400 nm above T_t .

To determine the shape and the size of the assemblies, transmission electron microscopy (TEM) measurements were carried out. TEM images for **1**, **2**, **4**, **5**, **6**, and **7** are shown in Figures 9a, S5a–c (Supporting Information), 9b, and S5d, respectively, together with the one for **3** in Figure 9c. In TEM images, spherical particles with polydispersity, whose diameters were in the range of 20–200 nm, were observed. Since the observed particles appeared to be filled on the inside, those might not be vesicles but globules. The large discrepancy between the diameters determined by DLS and TEM measurements might be due to dehydration under reduced pressure for preparing the sample and measuring the TEM image,^{11a} suggesting that the forming globules in water were soft and contained large amounts of water molecules. In the TEM image for **3**, transparent bundles with a diameter of 50–150 nm consisting of fibers with a diameter of ca. 10 nm were observed together with globular particles (Figure 9c). Although the origin of these globules is not clear yet, the observed globules might be considered to have formed in the preparation procedure of the sample. A scanning electron microscopy (SEM) image of a xerogel sample of **3** was also measured, revealing a network structure (Figure 9d).

Formation of Self-Assemblies. In these compounds, the self-assembly phenomena can be considered to be a subtle balance

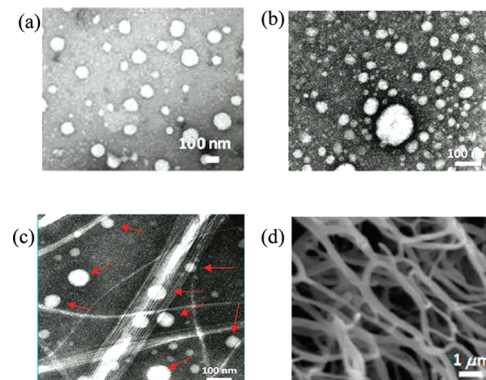


Figure 9. TEM images for **1** (a), **6** (b), and **3** (c) and SEM image for a xerogel of **3** (d). Red arrows indicate the globules.

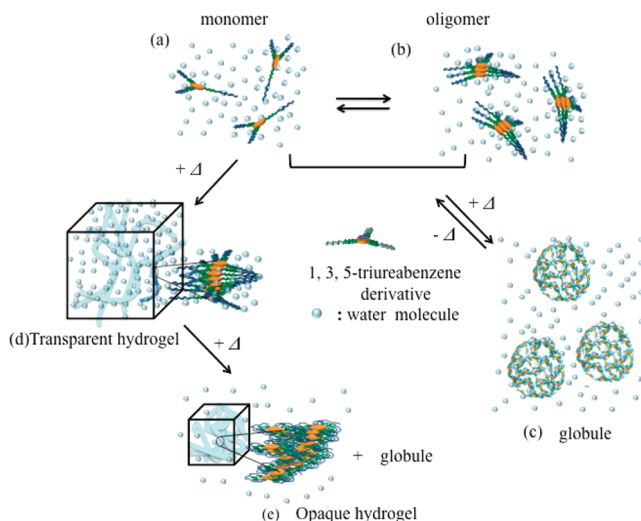


Figure 10. Schematic drawing of the formation of the globule and hydrogel.

between the hydrophobic (C_n) and hydrophilic (Eg_m) chains. The thermal response behavior was due to the property of the Eg_m chains, which increase the solubility of the molecule in water by the solvation of water molecules below the LCST and show a decrease of the solubility resulting from the dehydration above the LCST. Therefore, the T_t value of the LCST depends on the solubility of the compound in water and becomes higher with increasing solubility. In these compounds, the smaller the ratio (alkyl/Eg) of the lengths of the alkyl and Eg side chains, the higher the solubility of the molecule in water. In **1**, **2**, and **3**, the length of the alkyl chain varied in the order of C_6 , C_7 , and C_8 with a constant Eg_3 chain. The solubility in water thus decreased in the order of **1**, **2**, and **3**. This order is consistent with the result that T_t for **2** was lower than that for **1** at the same concentration. Similarly, the order of the solubilities of **4** and **5** having C_6 and C_8 with Eg_3 was **4** > **5**, suggesting that the T_t value for **4** would be higher than that for **5**. In addition, since **4** and **5** have tertiary amino groups undergoing protonation, the solubility varies depending on the pH of the aqueous solution. The T_t value shifted higher by the protonation of amine with decreasing pH. In contrast, **6** and **7** have Eg_3 and Eg_6 chains, respectively, with C_6 chains and alkyl/Eg ratios in the order of **6** > **7**, leading to the order of the solubility in water being **7** > **6**. The value of T_t for **7** was therefore higher than that for **6**. Since **6** and **7** also had amino groups, their T_t values also depended on the pH.

A schematic drawing of the formation of globules and a hydrogel is shown in Figure 10. As suggested by VT ^1H NMR and ESR spectra, below T_t of the LCST, the compounds except for **3** undergoing hydration of the surrounding water molecules were at equilibrium for an isolated monomer (Figure 10a) and small-sized assembly (oligomer) (Figure 10b), in which the latter was dominant with decreasing solubility. Above T_t of the LCST, the monomer and oligomer formed globular particles by decreasing the solubility (Figure 10d). The formation of globules and the turbidity took place simultaneously and the amount and/or size of the globule increased on warming. On the other hand, **3** formed a hydrogel (Figure 10c). For the formation of a hydrogel, primary, secondary, and tertiary assembly structures are generally required.²⁵ The benzene and urea groups might help to form a primary layered structure by $\pi-\pi$ interaction and hydrogen

bonding, respectively, and the alkyl and Eg chains might help to form the secondary and tertiary structures by the hydrophobic and hydrophilic interactions between the side chains. In the temperature dependence of UV spectra in the 0.2 mM sample, which was smaller than the MGC of 0.5 mM for **3**, although the blue shift of the absorption at 236 nm typical for an H-type aggregated structure^{15,19,26} was not observed, a broadening of the absorption and its red shift suggesting J-type aggregated structure was observed in the temperature range of 5–25 °C (Figure S6a, Supporting Information). In the IR spectrum¹⁹ for the xerogel, the characteristic absorptions of amido I and II at 1632 and 1569 cm^{-1} assigned as the urea hydrogen bond were observed (Figure S6b). The turbidity of the hydrogel for **3** before shrinking might be caused by the formation of globules, as observed by the appearance of the signals due to the globules in NMR spectra at 35 °C. The shrinking observed above 39 °C was considered to be due to the desorption of water molecules. An example of similar shrinking behavior of a gel was reported in the literature.^{6c}

CONCLUSION

In this study, we prepared 1,3,5-triureabenzene derivatives having amphiphilic side chains C_nEg_3 (**1**, **2**, and **3**, $n = 6, 7$, and 8, respectively), $C_n\text{NMEg}_3$ (**4** and **5**, $n = 6$ and 8, respectively), and $C_6\text{NTEg}_m$ (**6** and **7**, $m = 3$ and 6, respectively) and successfully observed LCST phenomena in pure water. LCST is a thermal behavior rare for small-sized molecules, especially in pure water. In the compounds except for **3** above the transition temperature, T_t , of the LCST, the formation of globular particles with polydispersity were observed on TEM images and the sizes of the globules were determined to be 2400–750 nm by DLS measurement. Compound **3**, however, formed a thermally reversed hydrogel with an MGC of 0.05 wt %. The LCST behaviors for all compounds were reversible in the cycle of warming and cooling, while the formation of the hydrogel by **3** was irreversible. It is worth noting that the structural difference between **2** and **3**, forming a globule and a hydrogel, respectively, was only one methylene unit in a side chain. In addition, the compounds containing the tertiary amino groups in the side chains responded to pH in the solution, and the values of T_t for **4**–**7** increased with decreasing pH of the solution. The response of T_t was highly sensitive to the pH of the solution compared with those for thermally responsive polymers reported previously.²⁷ Especially **5** and **6** showed high sensitivity of T_t to pH in the neutral region: **5**, $T_t = 55$ and 65 °C at pH 7.0 and 6.6, respectively; **6**, $T_t = 10$ and 25 °C at pH 7.0 and 6.3, respectively. In the solutions of **6** and **7** carrying a stable aminoxy, TEMPO, the water proton relaxivity, r_1 , showed large differences below and above T_t and the formation of globules above T_t reduced the r_1 value: **6**, $r_1 = 1.7$ and 0.24 $\text{mM}^{-1} \text{s}^{-1}$ at 10 and 25 °C, respectively; **7**, $r_1 = 0.90$ and 0.39 $\text{mM}^{-1} \text{s}^{-1}$ at 35 and 50 °C, respectively. Furthermore, in the solution of **6** at a constant temperature of 25 °C and at pH 6.0 and 7.0, at which the solution was clear and turbid, respectively, the r_1 values were 0.92 and 0.23 $\text{mM}^{-1} \text{s}^{-1}$, respectively. The obtained r_1 value at pH 6.0 was 4 times larger than that at pH 7.0.

The behavior of the formation and decomposition of the globules and the drastic change of the r_1 value caused by the small difference in pH of the solution can be considered as the switching function for the take-up and the release of the nanocapsules in the DDS⁹ and the amplification of detection sensitivity in MRI agents,²⁸ respectively. To control the size of self-assemblies, the preparation of analogous supramolecules having functional

groups is in progress. Furthermore, for more precise determination of the size of globules, cryo-TEM measurements are being designed.

■ ASSOCIATED CONTENT

Supporting Information. Experimental methods (S1), T_{r800} vs T plots for 4 at the given pH values (Figure S1), T_{r800} vs 10 and 30 °C plots for 3 (Figure S2), VT ^1H NMR spectra for 1 (a), 2 (b), 3 (c), 4 (d), and 5 (e) (Figure S3), ESR spectra at various temperatures for 7 (a) and TEMPO-OH (b) and signal intensity (c) and line width (d) vs T plots for 6 and 7 (Figure S4), TEM images for 2 (a), 4 (b), 5 (c), and 7 (d) (Figure S5), and (a) temperature dependence of UV spectra for 3 and (b) IR spectra for the xerogel of 3 (Figure S6). This material is available free of charge via the Internet at <http://pubs.acs.org>.

■ AUTHOR INFORMATION

Corresponding Author

*E-mail: koga@fc.phar.phyushu-u.ac.jp.

■ ACKNOWLEDGMENT

This work was supported by the Nanotechnology Support Project of the Ministry of Education, Culture, Sports, Science and Technology (MEXT), Japan.

■ REFERENCES

- (a) Gil, E. S.; Hudson, S. M. *Prog. Polym. Sci.* **2004**, *29*, 1173–1222. (b) Schmaljohann, D. *Adv. Drug Delivery Rev.* **2006**, *58*, 1655–1670. (c) Chilkoti, A.; Dreher, M. R.; Meyer, D. E.; Raucher, D. *Adv. Drug Delivery Rev.* **2002**, *54*, 613–630.
- (a) Kim, J. K.; Lee, E.; Lim, Y. B.; Lee, M. *Angew. Chem., Int. Ed.* **2008**, *47*, 4662–4666. (b) Lee, E.; Kim, J. K.; Lee, M. *Angew. Chem., Int. Ed.* **2009**, *48*, 3657–3660. (c) Sundararaman, A.; Stephan, T.; Grubbs, R. B. *J. Am. Chem. Soc.* **2008**, *130*, 12264–12265. (d) Kiyonaka, S.; Sugiyasu, K.; Shinkai, S.; Hamachi, I. *J. Am. Chem. Soc.* **2002**, *124*, 10954–10955.
- (a) Matsumoto, S.; Yamaguchi, S.; Ueno, S.; Komatsu, H.; Ikeda, M.; Ishizuka, K.; Iko, Y.; Tabata, K. V.; Aoki, H.; Ito, S.; Noji, H.; Hamachi, I. *Chem.—Eur. J.* **2008**, *14*, 3977–3986. (b) Hirose, T.; Matsuda, K.; Irie, M. *J. Org. Chem.* **2006**, *71*, 7499–7508.
- (a) Bae, Y.; Fukushima, S.; Harada, A.; Kataoka, K. *Angew. Chem., Int. Ed.* **2003**, *42*, 4640–4643. (b) Rodríguez-Hernández, J.; Lecommandoux, S. *J. Am. Chem. Soc.* **2005**, *127*, 2026–2027. (c) Du, J. Z.; Tang, Y. P.; Lewis, A. L.; Armes, S. P. *J. Am. Chem. Soc.* **2005**, *127*, 17982–17983. (d) Yusa, S.; Sugahara, M.; Endo, T.; Morishima, Y. *Langmuir* **2009**, *25*, 5258–5265.
- (a) Park, T. G.; Hoffman, A. S. *Macromolecules* **1993**, *26*, 5045–5048. (b) Liu, X.; Cheng, F.; Liu, H.; Chen, Y. *Soft Matter* **2008**, *4*, 1991–1994. (c) Luzon, M.; Boyer, C.; Peinado, C.; Corrales, T.; Whittaker, M.; Tao, L.; Davis, T. P. *J. Polym. Sci., Part A: Polym. Chem.* **2010**, *48*, 2783–2792.
- (a) Wang, X. H.; Qiu, X. P.; Wu, C. *Macromolecules* **1998**, *31*, 2972–2976. (b) Cheng, H.; Shen, L.; Wu, C. *Macromolecules* **2006**, *39*, 2325–2329. (c) Wu, X. S.; Hoffman, A. S.; Yager, P. *J. Polym. Sci., Part A: Polym. Chem.* **1992**, *30*, 2121–2129. (d) Maeda, Y.; Higuchi, T.; Ikeda, I. *Langmuir* **2000**, *16*, 7503–7509.
- (a) Feil, H.; Bae, Y. H.; Feijen, J.; Kim, S. W. *Macromolecules* **1993**, *26*, 2496–2500. (b) Dimitrov, I.; Trzebicka, B.; Müller, A. H. E.; Dworak, A.; Tsvetanov, C. B. *Prog. Polym. Sci.* **2007**, *32*, 1275–1343. (c) Chen, G.; Hoffman, A. S. *Nature* **1995**, *373*, 49–52.
- (a) Simmons, D. S.; Sanchez, I. C. *Macromolecules* **2008**, *41*, 5885–5889. (b) Sanchez, I. C. *Macromolecules* **1979**, *12*, 980–988. (c) Erman, B.; Flory, P. J. *Macromolecules* **1986**, *19*, 2342–2353. (d) Grosberg, A. Y.; Kuznetsov, D. V. *Macromolecules* **1992**, *25*, 1970–1979. (e) Tanaka, G.; Mattice, W. L. *Macromolecules* **1995**, *28*, 1049–1059.
- Kabanov, A. V.; Vinogradov, S. V. *Angew. Chem., Int. Ed.* **2009**, *48*, 5418–5429.
- (a) Yoshikawa, I.; Sawayama, J.; Araki, K. *Angew. Chem., Int. Ed.* **2008**, *47*, 1038–1041. (b) Hirose, T.; Matsuda, K. *Chem. Commun.* **2009**, *5832–5834*.
- (a) Betancourt, J. E.; Subramani, G.; Serrano-Velez, J. L.; Rosa-Molinari, E.; Rotello, V. M.; Rivera, J. M. *Chem. Commun.* **2010**, *46*, 8537–8539. (b) Betancourt, J. E.; Rivera, J. M. *J. Am. Chem. Soc.* **2009**, *131*, 16666–1668. (c) Lee, E.; Jeong, Y. H.; Kim, J. K.; Lee, M. *Macromolecules* **2007**, *40*, 8355–8360.
- (a) Richards, G. J.; Labuta, J.; Hill, J. P.; Mori, T.; Ariga, K. *J. Phys. Chem. Lett.* **2010**, *1*, 1336–1340. (b) Lee, S.; Lee, J.-S.; Lee, C. H.; Jung, Y.-S.; Kim, J.-M. *Langmuir* **2011**, *27*, 1560–1564.
- (a) Aathimakanand, S. V.; Savariar, E. N.; Thayumanavan, S. *J. Am. Chem. Soc.* **2005**, *127*, 14922–14929. (b) Kono, K.; Murakami, E.; Hiranaka, Y.; Yuba, E.; Kojima, C.; Harada, A.; Sakurai, K. *Angew. Chem., Int. Ed.* **2011**, *50* (28), 6332–6336.
- (a) Hayashi, H.; Karasawa, S.; Koga, N. *J. Org. Chem.* **2008**, *73*, 8683–8693. (b) Sato, Y.; Hayashi, H.; Okazaki, M.; Aso, M.; Karasawa, S.; Ueki, S.; Suemune, H.; Koga, N. *Magn. Reson. Chem.* **2008**, *46*, 1055–1058. (c) Hayashi, H.; Karasawa, S.; Tanaka, A.; Odoi, K.; Chikama, K.; Kurabayashi, H.; Koga, N. *Magn. Reson. Chem.* **2009**, *47*, 201–204.
- (a) Maeda, H. *Adv. Enzyme Regul.* **2001**, *41*, 189–207. (b) Bertini, I.; Bianchini, F.; Calorini, L.; Colagrande, S.; Fragai, M.; Franchi, A.; Gallo, O.; Gavazzi, C.; Luchinat, C. *Magn. Reson. Med.* **2004**, *52*, 669–672. (c) Lee, H.; Lee, E.; Kim, D. K.; Jang, N. K.; Jeong, Y. Y.; Jon, S. *J. Am. Chem. Soc.* **2006**, *128*, 7383–7389. (d) Besenius, P.; van den Hout, K. P.; Albers, H. M. H. G.; de Greef, T. F. A.; Olijve, L. L. C.; Hermans, T. M.; de Waals, B. F. M.; Bomans, P. H. H.; Sommerdijk, N. A. J. M.; Portale, G.; Palmans, A. R. A.; van Genderen, M. H. P.; Vekemans, J. A. J. M.; Meijer, E. W. *Chem.—Eur. J.* **2011**, *17*, 5193–5203.
- (a) de Greef, T. F. A.; Smulders, M. M. J.; Wolffs, M.; Schenning, A. P. H. J.; Sijbesma, R. P.; Meijer, E. W. *Chem. Rev.* **2009**, *109*, 5687–5754. (b) Palmans, A. R. A.; Meijer, E. W. *Angew. Chem., Int. Ed.* **2007**, *46*, 8948. (c) Stals, P. J. M.; Haveman, J. F.; Martín-Rapún, R.; Filié, C. F. C.; Palmans, R. A.; Meijer, E. W. *J. Mater. Chem.* **2009**, *19*, 124–130.
- Obert, E.; Bellot, M.; Bouteiller, L.; Andrioletti, F. *Lehen-Ferrenbach, C.; Boué, F. J. Am. Chem. Soc.* **2007**, *129*, 15601–15605.
- Albertazzi, L.; Storti, B.; Marchetti, L.; Beltram, F. *J. Am. Chem. Soc.* **2010**, *132*, 4207–4214.
- van Gorp, J. J.; Vekemans, J. A. J. M.; Meijer, E. W. *J. Am. Chem. Soc.* **2002**, *124*, 14759–14769.
- (a) Estroff, L. A.; Hamilton, A. D. *Chem. Rev.* **2004**, *104*, 1201–1218. (b) de Loos, M.; Feringa, B. L.; van Esch, J. H. *Eur. J. Org. Chem.* **2005**, *17*, 3615–3631. (c) Khatua, D.; Maiti, R.; Dey, J. *Chem. Commun.* **2006**, *4903–4905*. (d) Jung, J. H.; Shinkai, S.; Shimizu, T. *Chem.—Eur. J.* **2002**, *8*, 2684–2690. (e) Komatsu, H.; Matsumoto, S.; Tamaru, S.-i.; Kaneko, K.; Ikeda, M.; Hamachi, I. *J. Am. Chem. Soc.* **2009**, *131*, 5580–5585.
- (a) Mousseau, J. J.; Xing, L.; Tang, N.; Cuccia, L. A. *Chem.—Eur. J.* **2009**, *15*, 10030–10038. (b) Singh, T.; Kumar, A. *J. Phys. Chem. B* **2007**, *111*, 7873–7851.
- (a) Makarov, T. N.; Bagryanskaya, E. G.; Paul, H. *Appl. Magn. Reson.* **2004**, *26*, 197–211. (b) Atkins, P. W.; Kivelson, D. *J. Chem. Phys.* **1966**, *44*, 169–174.
- (a) Livramento, J. B.; Sour, A.; Borel, A.; Merbach, A. E.; Toth, V. *Chem.—Eur. J.* **2006**, *12*, 989–1003. (b) Yang, J. J.; Yang, J. H.; Wei, L. X.; Zurkiya, O.; Yang, W.; Li, S. Y.; Zou, J.; Zou, Y. B.; Maniccia, A. L. W.; Mao, H.; Zhao, F.-Q.; Malchow, R.; Zhao, S.-M.; Johnson, J.; Hu, X.-P.; Krogstad, E.; Liu, Z.-R. *J. Am. Chem. Soc.* **2008**, *130*, 9260–9267.
- (a) Winalski, C. S.; Shortkroff, S.; Mulkern, R. V.; Schneider, E.; Rosen, G. M. *Magn. Reson. Med.* **2002**, *48*, 965–972. (b) Cheng, Z.; Thorek, D. L. J.; Tsourkas, A. *Adv. Funct. Mater.* **2009**, *19*, 3753–3759.

(c) Shiraishi, K.; Kawano, K.; Maitani, Y.; Yokoyama, M. *J. Controlled Release* **2010**, *148*, 160–167.

(25) In *Molecular Gels, Materials with Self-Assembled Fibrillar Networks*; Weiss, R. A., Terech, P., Eds.; Springer: New York, 2006.

(26) (a) Hoebeek, F. J. M.; Wolffs, M.; Zhang, J.; De Feyter, S.; Leclère, P.; Schenning, A. P. H. J.; Meijer, E. W. *J. Am. Chem. Soc.* **2007**, *129*, 9819–9828. (b) Zhang, J.; Hoeben, F. J. M.; Pouderoijen, M. J.; Schenning, A. P. H. J.; Meijer, E. W.; De Schryver, F. C.; De Feyter, S. *Chem.—Eur. J.* **2006**, *12*, 9046–9055.

(27) (a) Li, L.-Y.; He, W.-D.; Li, W.-T.; Zhang, K.-R.; Pan, T.-T.; Ding, Z.-L.; Zhang, B.-Y. *J. Polym. Sci., Part A: Polym. Chem.* **2010**, *48*, 5018–5029. (b) Kang, M. K.; Kim, J.-C. *J. Appl. Polym. Sci.* **2010**, *118*, 421–427.

(28) (a) Weissleder, R.; Mahmood, U. *Radiology* **2001**, *219*, 316–333. (b) Querol, M.; Bogdanov, A., Jr. *J. Magn. Reson. Imaging* **2006**, *24*, 971–982.